Journal of Zhejiang University-SCIENCE A (Applied Physics & Engineering) 2025 26(3):212-225
www.jzus.zju.edu.cn; www.springer.com/journal/11582
E-mail: jzus_a@zju.edu.cn

Research Article

https://doi.org/10.1631/jzus.A2400013

Multi-field, time-varying behavior, and cracking mechanisms of early-age concrete in balastless track beds

Xiao LI[1,2], Juanjuan REN[1]✉, Shijie DENG[1], Zeyong ZHANG[1], Xueyi LIU[1]

[1]*MOE Key Laboratory of High-speed Railway Engineering, Southwest Jiaotong University, Chengdu 610031, China*
[2]*China MCC5 Group Corp. Ltd., Chengdu 610063, China*

Abstract: Cracking of early-age concrete can occur in the track beds of high-speed railways due to changes in material properties, environmental effects, and construction processes. This is a multi-field, time-varying issue involving hydro-thermo-chemo-mechanical coupling. However, to date, research has not adequately described the early-age cracking mechanisms in track beds, and few risk control measures have been proposed. To solve this problem, we incorporated the hydration degree of concrete into multi-field coupling equations for early-age concrete, and set boundary conditions that account for environmental influences and various stress factors that typically cause early creep of concrete. A four-field coupled risk prediction model was built based on hydro-thermo-chemo-mechanical properties, and was used to calculate and analyze various time-varying behavior (including the risk and form of cracking) in the hydro, thermo, chemo, and mechanical fields of early-age concrete. Finally, we focused on material-related factors (maximum heat of hydration and peak heat release time), environmental factors (temperature difference between day and night, average daily cooling rate, and intensity of solar radiation), and construction technique factors (molding temperature, pouring time, and thermal insulation coefficient). The influence of these factors on the early-age cracking risk of the track bed was analyzed, and risk control measures against early cracking were proposed accordingly.

Key words: Ballastless track; Early-age concrete; Hydro-thermo-chemo-mechanical coupling; Early cracking of track bed

1 Introduction

By the end of 2024, China's railway system had an operating mileage of over 162000 km, including 48000 km designated for high-speed rail. Ballastless tracks are important for high-speed railways due to their smoothness, stability, and low maintenance requirements (Ren et al., 2023). China has formed a ballastless track ecosystem comprising five types: the CRTS I and II double-block types and the CRTS I, II, and III slab types (Ren et al., 2021). Thanks to its simple structure, accurate and stable force transmission, and simple construction process, the CRTS I double-block track covers the most existing mileage in China and has become the most popular foundation for new lines. Its structural form is detailed in Section S1 of the electronic supplementary materials (ESM).

For CRTS I double-block tracks, cracking in the cast-in-place, early-age concrete of track beds is typically caused by material degradation, unfavorable construction environments, and poor construction techniques. For the track beds or sleepers, cracking may occur between existing and newly-poured concrete, which can form irregularly on the surface of the track beds or regularly on the body of the track beds (Fig. 1). In areas of extreme climate such as mountains, deserts, or hot and humid regions, the risk of cracking is greater (particularly in the track beds), which may cause damage to the track structure and threaten its service life.

Early-age cracking of the track beds is not caused by external loads but is the result of shrinkage induced by changes in temperature and humidity. This shrinkage is a multi-field, time-varying process that couples hydration, heat, humidity, and force, and is also affected by material properties and environmental conditions (Miao, 2018). However, current research

✉ Juanjuan REN, jj.ren@swjtu.edu.cn
Xiao LI, https://orcid.org/0009-0005-3446-473X
Shijie DENG, https://orcid.org/0009-0006-4883-6888
Zeyong ZHANG, https://orcid.org/0009-0001-6793-6036

Received Jan. 7, 2024; Revision accepted Mar. 12, 2024;
Crosschecked Dec. 24, 2024

Fig. 1 Cracking in the track bed concrete

on the cracking of early-age concrete track beds is limited to single metrics, namely temperature or humidity (Zhang et al., 2013; Hu et al., 2018), which is insufficient for analyzing cracking mechanisms in complex scenarios. We summarized the current state of research on the multi-field behavior of early-age concrete, and evaluated the applicability and limitations of existing methods in Section S2 of the ESM.

Although existing studies have attempted to reveal the cracking mechanisms of early-age concrete structures through hydro-thermo-chemo-mechanical coupling models, these measures only suit simple structures that are less affected by environmental conditions. Thus, they lack the complexity needed to analyze double-block ballastless tracks (van Breugel, 1995; de Schutter, 2002; Gawin et al., 2006). Overall, there is a clear need for a model that can adequately describe the time-varying behavior and cracking mechanisms in such track beds, which would enable accurate risk forecasting for early-age concrete cracking and better formulation of risk control measures.

2 Risk prediction model for early-age concrete cracking

To better represent the influence of material properties, environmental conditions, and construction processes on the cracking of early-age concrete, we used the hydro-thermo-chemo-mechanical coupling theory to establish multi-field coupling control equations and boundary conditions. Through these, we developed a feasible expression for the risk coefficient of cracking.

2.1 Calculation method for the hydration field of early-age concrete in track beds

Considering the influence of temperature and humidity on the hydration rate of concrete, the hydration field of early-age concrete in the track bed can be expressed as (Cervera et al., 2002):

$$\frac{\partial \alpha}{\partial t} = A_{25}\beta_{\varphi}\beta_{T}, \tag{1}$$

where α is the degree of hydration; t is the time; A_{25} is the chemical affinity of the track bed concrete at the reference temperature of 25 °C; β_{φ} and β_{T} are the influence coefficients of humidity φ and temperature T, respectively. Since there are many existing studies on concrete hydration fields, a more detailed explanation of the parameters in Eq. (1) can be found in Section S3 of the ESM. Essentially, the temporospatial distribution of hydration degree in the trackage beds is caused by the uneven temporospatial distribution of temperature and relative humidity. There is no diffusion process in the hydration field itself, and there is no exchange occurring with the external environment. Therefore, the only definite solution condition of the hydration field is the initial hydration degree. In this study, we consider this to be the hydration degree when the track bed concrete enters the mold. Since the track bed concrete needs to be transported and poured into the mold before the initial setting, the initial hydration degree of the track beds is taken as 0.01.

2.2 Calculation method for the temperature field of early-age concrete in track beds

Assuming the heat conduction inside the concrete is isotropic and applying the law of conservation of energy, the governing equation for the micro-element temperature field inside the track is:

$$(\rho C)_{\text{eff}}\frac{\partial T}{\partial t} + \nabla\cdot(\lambda\nabla T) + \frac{\partial Q_{\text{h}}}{\partial t} = 0, \tag{2}$$

where $(\rho C)_{\text{eff}}$ is the equivalent volumetric heat capacity of the concrete; λ is the thermal conductivity; Q_{h}

is the hydration heat release of the cement gelling system. A more detailed discussion of these parameters is provided in Section S4.1 of the ESM.

For our model, we consider the initial time as the moment that the track bed concrete enters the mold. Therefore, the initial temperature is the spatially distributed temperature of each track component at the time of molding. Convective heat transfer, solar radiation, radiative heat transfer, and water evaporation are the main forms of heat exchange between the early-age track beds and the external environment. The above boundary conditions of the temperature field are discussed further in Section S4.2 of the ESM.

2.3 Calculation method for the humidity field of early-age concrete in track beds

Following the law of conservation of mass, transported water and water consumed during concrete hydration need to be considered. The controlling equation for the humidity field of concrete is therefore established as:

$$\frac{\mathrm{d}w_{\mathrm{e}}}{\mathrm{d}t}+\frac{\mathrm{d}w_{\mathrm{n}}}{\mathrm{d}t}+\nabla\cdot D_{\mathrm{w}}\zeta_{\varphi}\nabla\varphi+\nabla\cdot\delta_{\mathrm{p}}\nabla(\varphi P_{\mathrm{sat}})=0, \quad (3)$$

where w_{e} is the the amount of water stored in mature concrete; w_{n} is the mass of consumed (bound) water (kg/m^3); D_{w} is the diffusion coefficient of concrete's relative humidity (m/s^2); ζ_{φ} is the function of water storage, which represents the relationship between relative humidity and free water content; δ_{p} is the vapor diffusion coefficient in concrete (kg/(m·s·Pa)); P_{sat} is the saturated vapor pressure at temperature T (Pa). Bound water content is expressed as a function of the degree of hydration:

$$w_{\mathrm{n}}=0.25m_{\mathrm{c}}\alpha, \quad (4)$$

where m_{c} represents the mass of cement contained in the unit volume of concrete in the track bed.

The two main factors affecting the relative humidity in concrete are the free water content and the porous structure. For the former factor, it is intuitive that the higher the free water content, the greater the relative humidity. For the latter, the influence on relative humidity is multifaceted: i) the larger the porosity, the higher the free water content under the saturated state of relative humidity; ii) the free water in concrete mainly resides in the gel pores and capillary pores. This means the free water in the gel pores can approach humidity saturation when the relative humidity is 50% and is difficult to lose; concordantly, the water content in the capillary pores is low when the relative humidity is 50%, but increases rapidly as the relative humidity increases (Fig. 2).

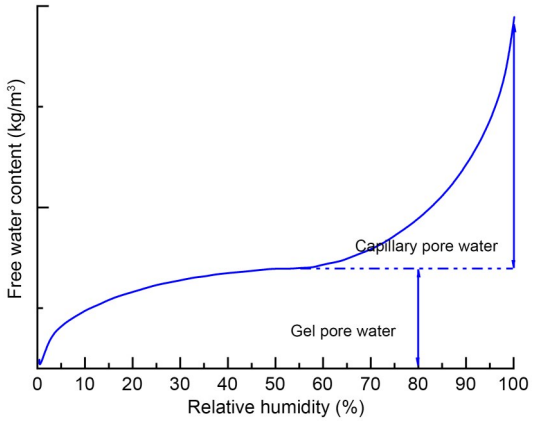

Fig. 2 Relationship between relative humidity and free water content

For a mature sleeper or supporting layer, the pore structure is stable, and in most cases, the relative humidity in the concrete will not drop below 50%. According to Künzel (1995), the amount of water stored in mature concrete can be expressed as a function of relative humidity and volumetric water content:

$$w_{\mathrm{e}}=w_{\mathrm{f}}\frac{(b-1)\varphi}{b-\varphi}, \quad (5)$$

where w_{f} is the saturated water content of the relative humidity of the mature concrete sleeper or supporting layer (kg/m^3). Higher concrete strength (or smaller water-cement ratio) corresponds to smaller internal porosity of concrete and lower saturated water content. b is the dimensionless factor that characterizes the proportion of gel pores inside the concrete. This factor is always greater than 1 and increases with a higher proportion of gel pore space.

The porosity and hydration degree in early-age concrete have a roughly linear relationship, and the proportion of gel pores also increases gradually with the hydration degree. From this, expressions for free water content, relative humidity, and degree of hydration can be established. Using the water storage

function (Eq. (5)) for mature concrete, the saturated water content of early-age track concrete (w_f) and the dimensionless factor representing the ratio of gel pores (b) are expressed as:

$$w_f(\alpha) = w_{fu} + \frac{(w_{f0} - w_{fu})}{\alpha_u}(\alpha_u - \alpha), \tag{6}$$

$$b = b_0 + n_b \exp(m_b \alpha), \tag{7}$$

where w_{f0} is the free water content of the initially-mixed track bed concrete, which is taken as the mass of the mixed water (kg/m^3); w_{fu} is the saturated free water content (kg/m^3) when the track bed reaches the final degree of hydration; α_u is the final hydration degree; b_0, n_b, and m_b are the correction coefficients for the dimensionless factor b for early-age concrete, and can be obtained by back-calculating the parameters from the relative humidity evolution curve during the hydration of sealed concrete.

The relative humidity diffusion coefficient is the key factor for determining the moisture transmission capacity of concrete and calculating the humidity field. It largely depends on the porosity and relative humidity inside the concrete. The pore structure in mature concrete is fully formed and unlikely to change, meaning the relative humidity diffusion coefficient is only affected by the relative humidity. Typically, numerical calculation of the humidity field in early-age concrete uses the relative humidity diffusion coefficient of mature concrete, and does not consider how changes in pore structure affect this coefficient during the hydration process. However, this approach will underestimate the humidity transmission rate for early-age concrete, as well as the rate of water loss under dry conditions. Instead, we consider the correlation between the hydration degree in early-age concrete and the pore structure, and also incorporate the relative humidity diffusion coefficient of mature concrete, to establish a more refined expression for the coefficient of early-age concrete:

$$D_w = D_1^{\infty} \times 10^{n_D(1-\alpha)} \left[0.05 + \frac{1 - 0.05}{1 + \left(\frac{1-\varphi}{1-\varphi_c} \right)^{n_\varphi}} \right], \tag{8}$$

where D_w is the relative humidity diffusion coefficient; D_1^{∞} is the permeability coefficient of mature track bed concrete under a saturated humidity state (m^2/h); φ_c is the relative humidity when the relative humidity diffusion coefficient is $0.5D_1^{\infty} \times 10^{n_D(1-\alpha)}$; n_D is the influence index of hydration degree on the relative humidity diffusion coefficient, which is about 6 to 10 (Du, 2015); n_φ is the curve fitting index of relative humidity diffusion coefficient. These parameters depend on the specific concrete mixing ratio and can usually be obtained through material drying tests. A smaller porosity value will result in a denser pore structure and a smaller water permeability coefficient D_1^{∞}. By the CEB-FIP recommendations (CEB, 1990), the D_1^{∞} of the supporting layer and sleeper are set as 2.0×10^{-6} m^2/h and 0.6×10^{-6} m^2/h , respectively, i.e., φ_c=0.8 and n_φ=15.

Present research does not typically account for vapor diffusion in the numerical modeling of humidity fields for early-age concrete, despite its importance for moisture transport in concrete. For mature concrete with a stable pore structure, the vapor diffusion coefficient can be expressed as:

$$\delta_p = \frac{T^{0.81}}{\mu P_A} \times 2.0 \times 10^{-7}, \tag{9}$$

where P_A is the standard atmospheric pressure (Pa); μ is the resistance factor of water vapor diffusion in concrete.

The resistance factor of water vapor diffusion largely depends on the internal pore structure of the concrete. Typically, in mature concrete, it ranges from 200 to 300 (Künzel, 1995), with a higher concrete strength corresponding to a greater value.

During the hydration process of the early-age track bed concrete, the internal porosity of the concrete gradually decreases and the structure becomes denser, causing an increase in the resistance factor of water vapor diffusion μ in line with the degree of hydration. Current research on the resistance factor of water vapor diffusion considers various concrete materials (although none specifically for early-age concrete) and has shown that the resistance factors for different materials are on the same order of magnitude. Considering the fact that the porosity decreases linearly as hydration develops in early-age concrete, we propose the following function to account for the degree of hydration:

$$\mu = \mu_0(1 + n_\mu \alpha), \tag{10}$$

where μ_0 is the initial resistance factor of water vapor diffusion, which can be taken as 30 to 50; n_μ is the correction coefficient for water vapor diffusion resistance factor.

The initial time condition is when the track bed concrete is poured into the mold. According to our assumed initial conditions for the hydration and temperature fields, there is a strict time window between mixing and pouring of the track bed concrete, in which the water consumed in hydration and lost in drying is limited. Therefore, we assume that the initial relative humidity of the humidity field is 100%. To account for the water added to the sleeper and supporting layer before pouring, as well as the dry environment and humidity diffusion of the supporting layer itself, we assume that the relative humidity of the sleeper and the supporting layer is 90% when the track bed is poured. The humidity field is generally described by two boundary conditions: the water evaporation and the wet surface, both of which are discussed in detail in Section S5 of the ESM.

2.4 Calculation method for the mechanical field of early-age concrete in track beds

For mature sleepers and supporting layers, which can be regarded as elastic bodies unaffected by time, the mechanical parameters such as elastic modulus and Poisson's ratio are stable, and the creep is minimal. Their mechanical field follows the classical elastic calculation method, using 3D displacement as the field variable:

$$\boldsymbol{u}=\boldsymbol{u}(x,y,z,t), \tag{11}$$

where $\boldsymbol{u}$ is three-dimensional displacement field.

After the concrete is poured, the track bed gradually solidifies, with elastic modulus, tensile strength, creep, and other mechanical characteristics all showing a strong correlation with the degree of hydration. In these early stages, track bed creep is affected by factors such as hydration and stress state, and in turn impacts the stress evolution, forming a complex coupling relationship. Therefore, a more realistic early-age field calculation method is needed, in which the coupling of the mechanical field and creep is considered.

Accordingly, we adopt the stress increment algorithm and the rate-type creep law in calculating the mechanical field. Here, the creep is assumed to be incremental and is treated similarly to other external strains, such as those caused by temperature and humidity. The mechanical field of the early-age track bed is a vector field, with the variables being the 3D displacement and creep strain vectors:

$$\boldsymbol{\varepsilon}_\mathrm{c}=\boldsymbol{\varepsilon}_\mathrm{c}(x,y,z,t), \tag{12}$$

where $\boldsymbol{\varepsilon}_\mathrm{c}$ is the creep strain vector.

The early-age track bed gradually acquires strength and elastic modulus with higher hydration, reflecting the properties of solid materials. Its mechanical properties can be expressed through the degree of hydration (de Schutter and Taerwe, 1996):

$$\begin{aligned}
E(\alpha)&=E\left(\frac{\alpha-\alpha_0}{\alpha_\mathrm{u}-\alpha_0}\right)^{\beta_E},\\
f_\mathrm{t}(\alpha)&=f_\mathrm{t}\left(\frac{\alpha-\alpha_0}{\alpha_\mathrm{u}-\alpha_0}\right)^{\beta_\mathrm{t}},\\
f_\mathrm{c}(\alpha)&=f_\mathrm{c}\left(\frac{\alpha-\alpha_0}{\alpha_\mathrm{u}-\alpha_0}\right)^{\beta_\mathrm{c}},
\end{aligned} \tag{13}$$

where $E(\alpha)$, $f_\mathrm{t}(\alpha)$, and $f_\mathrm{c}(\alpha)$ are the elastic modulus, tensile strength, and compressive strength, respectively, of the early-age track bed concrete for a degree of hydration α; E, f_t, and f_c are the elastic modulus, tensile strength, and compressive strength, respectively, at the peak hydration degree; β_E, β_t, and β_c are the exponential constants of the elastic modulus, tensile strength, and compressive strength, respectively; α_0 is the degree of hydration at the time of final setting.

Since early-age concrete is unlikely to experience compression failure, tensile strength is a common mechanical indicator used to evaluate its crack resistance. We consider its standard value f_t as 2.39 MPa, which defines the tensile strength of the C40 concrete on the 28 d aged concrete, and set the elastic modulus E as 32.50 GPa, in accordance with the Code for Design of Concrete Structures (MOHURD, 2004). Referring to the existing test results (de Schutter and Taerwe, 1996), the hydration degree at the final setting is taken as 0.20, and the exponential constants β_E and β_t are taken as 0.60 and 1.00, respectively.

The confinement stress of the early-age concrete track bed suggests a strong temporal correlation, and the deformation mainly consists of the instantaneous

reversible elastic strain ε_e, the creep strain ε_c, the humidity strain ε_φ, and the temperature strain ε_T. The constitutive relation of the incremental stress–strain formula is expressed by the following differential equation:

$$\dot{\boldsymbol{\sigma}}=\boldsymbol{D}_c(\alpha):\dot{\boldsymbol{\varepsilon}}_e=\boldsymbol{D}_c(\alpha):(\dot{\boldsymbol{\varepsilon}}-\dot{\boldsymbol{\varepsilon}}_c-\dot{\boldsymbol{\varepsilon}}_\varphi-\dot{\boldsymbol{\varepsilon}}_T), \tag{14}$$

where $\boldsymbol{\sigma}$ is the stress tensor; $\boldsymbol{D}_c(\alpha)$ is the stiffness matrix; $\boldsymbol{\varepsilon}$ is the strain tensor.

The temperature strain ε_T can be expressed as the product of the thermal expansion coefficient α_T and the temperature difference ΔT:

$$\varepsilon_T=\alpha_T\Delta T. \tag{15}$$

Once the concrete sets, it will shrink due to continuous hydration of its gel material (autogenous shrinkage) and environmental influence (drying-led shrinkage). Zhang et al. (2010) proposed that both autogenous and drying shrinkage can be regarded as humidity deformation caused by humidity drop, which is expressed as:

$$\varepsilon_\varphi=\varepsilon_c+\alpha_\varphi\Delta\varphi, \tag{16}$$

where α_φ is the humidity deformation coefficient.

To represent the early cracking of concrete and obtain an accurate restraint stress value, we must consider both temperature and humidity deformation, as well as the effects of creep and restraint stress relaxation under the influence of multiple factors. Accordingly, we utilize the strain superposition method, where creep is regarded as an external strain similar to temperature or humidity strain, and the dependent variable is calculated from the state of stress. The development of stress is then determined by the state of strains (e.g. creep), thus forming a calculation method that couples creep and stress.

The early-age concrete creep vector includes the recoverable short-term creep vector $\boldsymbol{\varepsilon}_{kv}$ and the irrecoverable long-term creep vector $\boldsymbol{\varepsilon}_{am}$. The one-dimensional model consists of a viscoelastic body and a viscous body in series, to reflect the recoverable creep and non-recoverable creep of the early-age concrete, respectively (de Schutter, 1999). The one-dimensional model of short-term creep can be expressed as:

$$E_{kv}(\alpha)(\boldsymbol{\varepsilon}_{kv}+\tau\dot{\boldsymbol{\varepsilon}}_{kv})=\boldsymbol{\sigma}, \tag{17}$$

where $E_{kv}(\alpha)$ is the elastic modulus of viscoelastic bodies; τ is the relaxation time of viscoelastic bodies.

In addition to the aging effects, stress states (such as tension or compression), stress level, and multi-axial stress behavior all affect early creep development. A more detailed description of factors affecting the creep can be found in Section S6 of the ESM. Utilizing the above equations and materials from the ESM, we can express the creep as follows:

$$\frac{\partial}{\partial t}\begin{bmatrix}\varepsilon_x^{am}\\ \varepsilon_y^{am}\\ \varepsilon_z^{am}\\ \varepsilon_{xy}^{am}\\ \varepsilon_{yz}^{am}\\ \varepsilon_{zx}^{am}\end{bmatrix}=\frac{1}{\eta_{am}(\alpha)}\begin{bmatrix}1&-\nu_c&-\nu_c&0&0&0\\ -\nu_c&1&-\nu_c&0&0&0\\ -\nu_c&-\nu_c&1&0&0&0\\ 0&0&0&2(1+\nu_c)&0&0\\ 0&0&0&0&2(1+\nu_c)&0\\ 0&0&0&0&0&2(1+\nu_c)\end{bmatrix}\begin{bmatrix}\beta_{am}\sigma_x\beta_{\sigma_x}\\ \beta_{am}\sigma_y\beta_{\sigma_y}\\ \beta_{am}\sigma_z\beta_{\sigma_z}\\ \sigma_{xy}\beta_{\sigma_{xy}}\\ \sigma_{yz}\beta_{\sigma_{yz}}\\ \sigma_{zx}\beta_{\sigma_{zx}}\end{bmatrix}, \tag{18}$$

$$E_{kv}(\alpha)\begin{bmatrix}\varepsilon_x^{kv}\\ \varepsilon_y^{kv}\\ \varepsilon_z^{kv}\\ \varepsilon_{xy}^{kv}\\ \varepsilon_{yz}^{kv}\\ \varepsilon_{zx}^{kv}\end{bmatrix}+\tau\frac{\partial}{\partial t}\begin{bmatrix}\varepsilon_x^{kv}\\ \varepsilon_y^{kv}\\ \varepsilon_z^{kv}\\ \varepsilon_{xy}^{kv}\\ \varepsilon_{yz}^{kv}\\ \varepsilon_{zx}^{kv}\end{bmatrix}=\begin{bmatrix}1&-\nu_c&-\nu_c&0&0&0\\ -\nu_c&1&-\nu_c&0&0&0\\ -\nu_c&-\nu_c&1&0&0&0\\ 0&0&0&2(1+\nu_c)&0&0\\ 0&0&0&0&2(1+\nu_c)&0\\ 0&0&0&0&0&2(1+\nu_c)\end{bmatrix}\begin{bmatrix}\sigma_x\\ \sigma_y\\ \sigma_z\\ \sigma_{xy}\\ \sigma_{yz}\\ \sigma_{zx}\end{bmatrix}, \tag{19}$$

where $\boldsymbol{\sigma}_i(i=x,y,z,xy,yz,zx)$ is the component of stress vector; $\eta_{am}(\alpha)$ is the coefficient of viscosity of viscous body; β_{am} is the correction coefficients for early-age concrete creep under tensile/compressive state; ν_c is Poisson's ratio of creep; β_{σ_i} is the correction coefficient of stress level for irrecoverable long-term creep;

ε_i^{am} and ε_i^{kv} ($i=x, y, z, xy, yz, zx$) is the component of recoverable short-term creep vector and irrecoverable long-term creep vector, respectively.

2.5 Numerical modeling

To simulate the continuous double-block track structure on the subgrade, the model length spans two sleepers with symmetrical boundaries in the longitudinal direction. In essence, we design a finite element model that couples multiple fields for the C40 track bed, the C60 sleeper, and the C20 hydraulic supporting layer. The interfaces between the new and old concrete and the surface area of the track bed, which exchange heat and humidity with the environment, are meshed and divided (Fig. 3) with a minimum mesh thickness of about 4 mm. More complete information on the validation and the calculation parameters of the model is provided in Section S7 of the ESM.

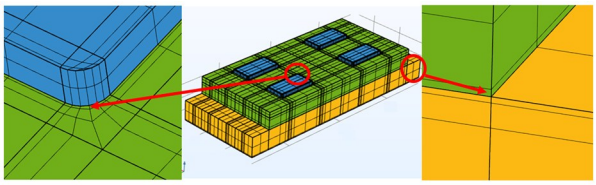

Fig. 3 Multi-field coupling model of an early-age double-block ballastless track

Field investigations suggest that cracks in early-age track bed concrete generally appear and spread within seven days after pouring, and are primarily concentrated in areas A and B (Fig. 4) near the four corners of the double-block sleeper (area A is on the inner side of the track; area B is near the outer side the track). The cracks in both A and B mainly originate at the corners of the sleeper and spread outward in a direction close to 45°. To explore the hydration degree, humidity, temperature, and stress development of the early-age track bed, ten calculation points are selected in the numerical model. Points 1–3 are in the inward-facing corner of area A. They are 10 cm horizontally from the corner of the sleeper, with vertical depths of 1, 13, and 25 cm, which represent the surface, the center, and the bottom layer of the inner side of the track bed, respectively. Points 4–6 are located in the inward-facing corner of area B and represent the surface, the center, and the bottom layer of the outer side of the track bed. Their horizontal distances from the corner of the sleeper and their vertical depths are the same as for points 1–3. Points 7–9 are in areas D, E, and C, respectively, 2 mm away from the side of the sleeper, and 1 cm deep. Point 10 is located deeper in the center of the sleeper, with a depth of 13 cm from the surface of the track bed. The locations of all calculation points are shown in Fig. 4.

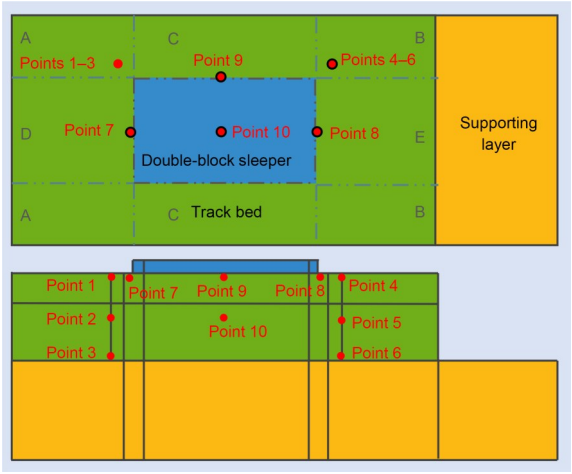

Fig. 4 Layout of the monitoring points in the numerical model

3 Multi-field time-varying behavior of early-age concrete track bed

We make the following assumptions in our model: the track bed is cast in place at 22:00; the initial hydration degree is 0.01; the pouring temperature of the concrete is 20 °C; the relative humidity is 100%. After the concrete has been cast in place for 4 h, it is covered and cured. The equivalent heat transfer coefficient between the track bed and the environment is 10, the solar radiation coefficient is 0.2, and the blackness coefficient is 0.1. To ensure the results reflect typical daily cycles, the ambient temperature, ambient relative humidity, and solar radiation intensity are represented by simple periodic functions, as shown in Fig. 5. The daily mean temperature is set as 20 °C, and the diurnal temperature difference is set as 6 °C, with the highest and lowest temperatures occurring at 4:00 and 16:00, respectively; the daily average relative humidity of the environment is set as 80%, and the relative day-to-night humidity difference is set as 20%, with the highest and lowest relative humidity occurring at 4:00 and 16:00, respectively; finally, the maximum intensity of solar radiation from 6:00 to 18:00 is set as 600 W/m^2.

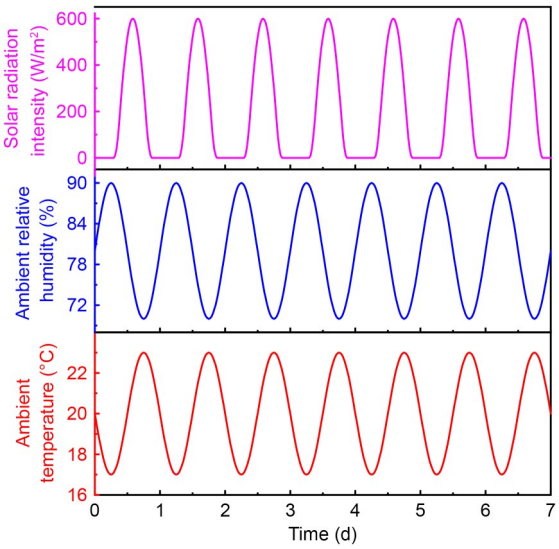

Fig. 5 External environmental conditions of the model

3.1 Time-varying development of the hydration degree

Fig. 6 shows the time dependence of hydration at various depths in the track bed for the first 7 d after casting. We can see the degree of hydration reaches 0.65 after 7 d, which is about 90% of the final hydration degree (α_u=0.76). The degree and rate of hydration at different depths in the track bed exhibit similar development trends, though the hydration rate at point 1 (on the surface) fluctuates with the ambient temperature. Also, the max spatial difference in the development of hydration degree during the first day is roughly 14%. The hydration development is particularly rapid on the first day (7 h after casting) with a maximum hydration rate of about 0.70 d^{-1}, after which the hydration rate decreases to about 0.05 d^{-1} on the 2nd and 3rd day, and then plateaus on the 7th day, while the track bed finally sets about 9.5 h after pouring.

3.2 Time-varying development of the temperature field

From these calculations, we obtained time-varying curves that represent the temperature at different points in the track bed for 7 d after casting (Fig. 7). Due to hydration heat release and heat exchange with the environment, the temperature of the early-age track bed is higher than the ambient temperature, but displays a diurnal cycle like that of ambient temperature. The highest temperature in the early-age track bed appears

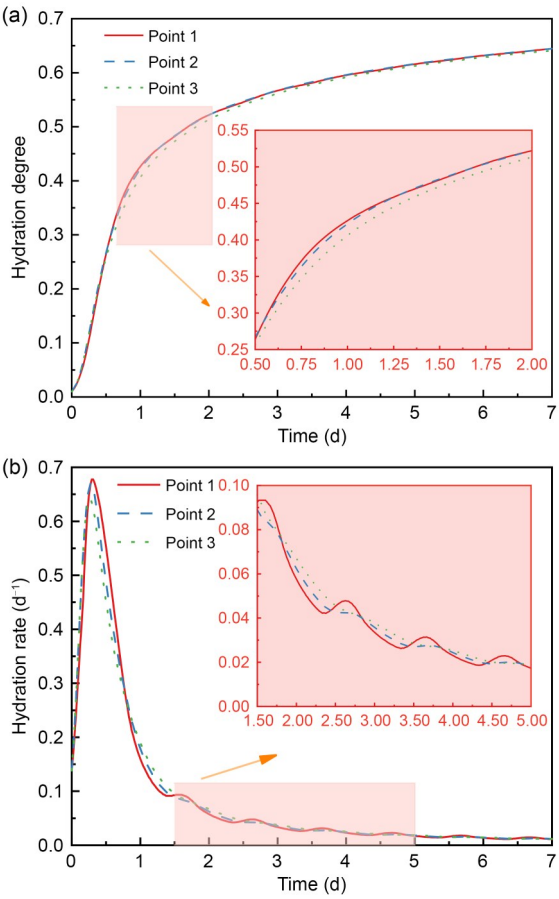

Fig. 6 Time evolution of the track bed's hydration field: (a) hydration degree; (b) hydration rate

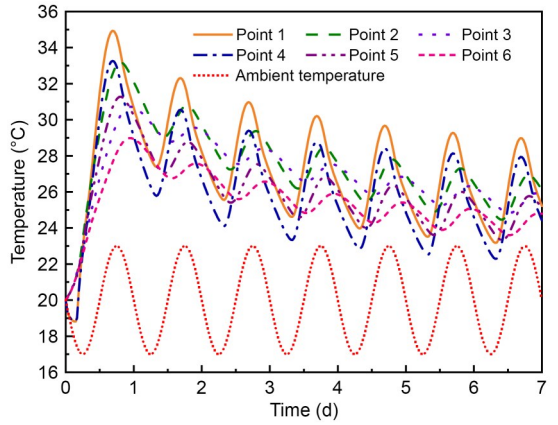

Fig. 7 Time evolution of temperature for measuring points in the track bed and the environment

12 to 24 h after pouring, and the highest temperature at point 1 (35 °C) occurs 16 h after pouring, which is 15 °C higher than the molding temperature. As the concrete ages, the peak temperature in the track bed decreases until it reaches the ambient temperature.

Intuitively, areas close to the surface experience a greater temperature difference between day and night, in addition to a faster change rate of temperature. The temperature inside the track bed shows an uneven distribution, with more complex behavior in the sides due to more heat dissipation pathways. As a result, the temperatures at these positions are lower than the internal temperatures at the same height. For example, the temperatures of points 4–6, measured on the outer side of the track bed, are lower than the temperatures of points 1–3, measured on the inner side of the track bed at the same height.

Since the track bed temperature changed significantly within one day after pouring, we extracted the temperature distribution cloud map of the double-block track at two time points: 12 h and 24 h. These results are shown in Fig. 8. Because the embedded sleeper destroys the integrity of the track bed, the temperature around the sleeper is then unevenly distributed. As for the temperature underneath the sleeper, it is significantly lower than that in other areas, which is caused by concurrent heat dissipation to the sleeper and the supporting layer.

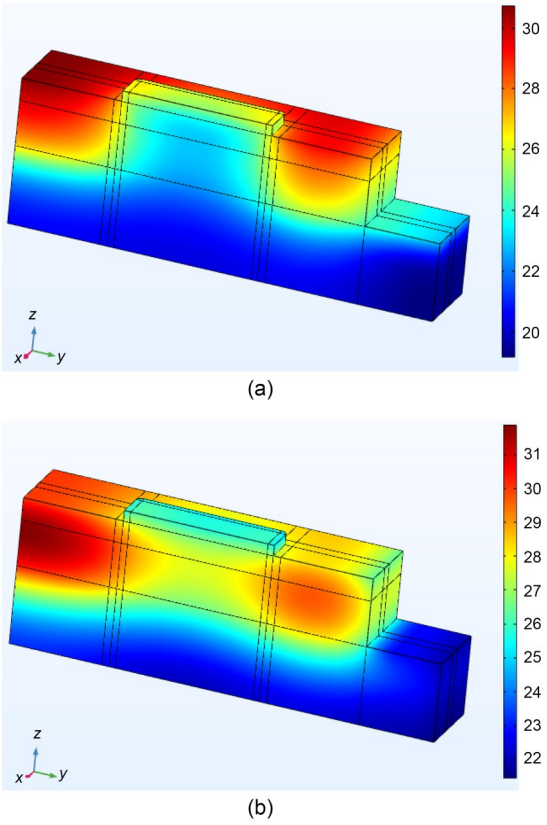

Fig. 8 Temperature (°C) cloud maps of key time points after pouring: (a) 12 h; (b) 24 h. References to color refer to the online version of this figure

3.3 Time-varying development of the humidity field

Fig. 9 shows the temporal evolution of free water content and relative humidity at points 1–3 in the track bed after casting. Fig. 10 displays the spatial distribution of relative humidity in the track bed on day 1 and day 7 after casting.

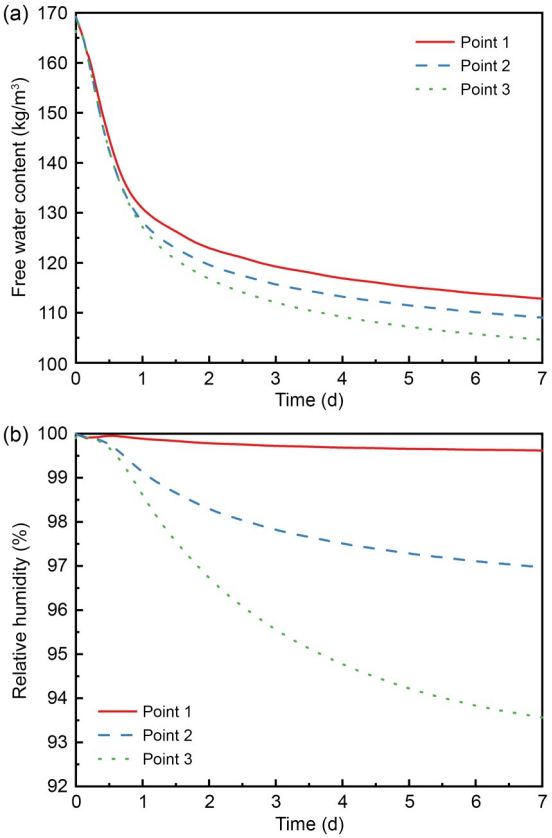

Fig. 9 Temporal evolution of the humidity field: (a) free water content; (b) relative humidity

The relative humidity and free water content in the track bed decrease over time, and the water consumption by hydration is the fastest within one day of pouring, but also slows down with time. Since the water storage capacity and humidity diffusion capacity at the sleeper are lower than that at the supporting layer, the spatial distribution of the relative humidity of the track bed is more affected by the drying of the supporting layer than that of the sleepers. The relative humidity change is most significant between the bottom of the track bed and the upper part of the supporting

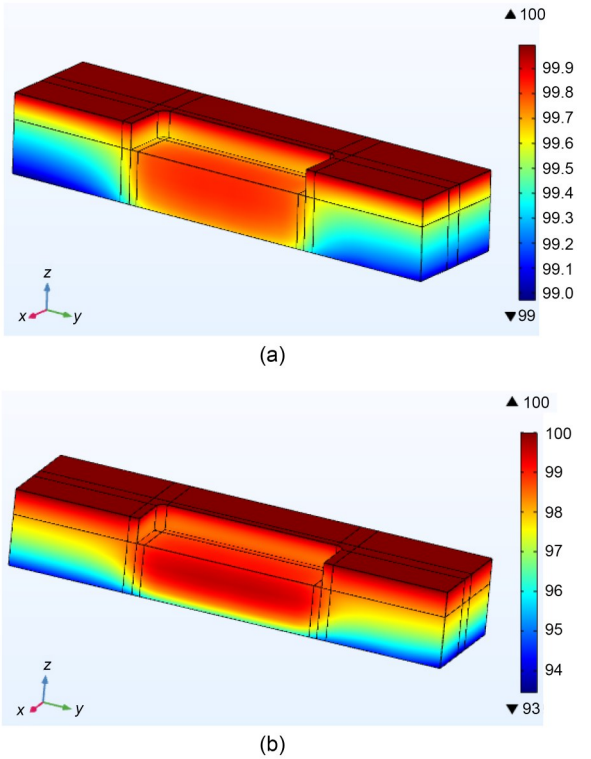

Fig. 10 Spatial distribution of relative humidity (%) in the track bed: (a) day 1; (b) day 7. References to color refer to the online version of this figure

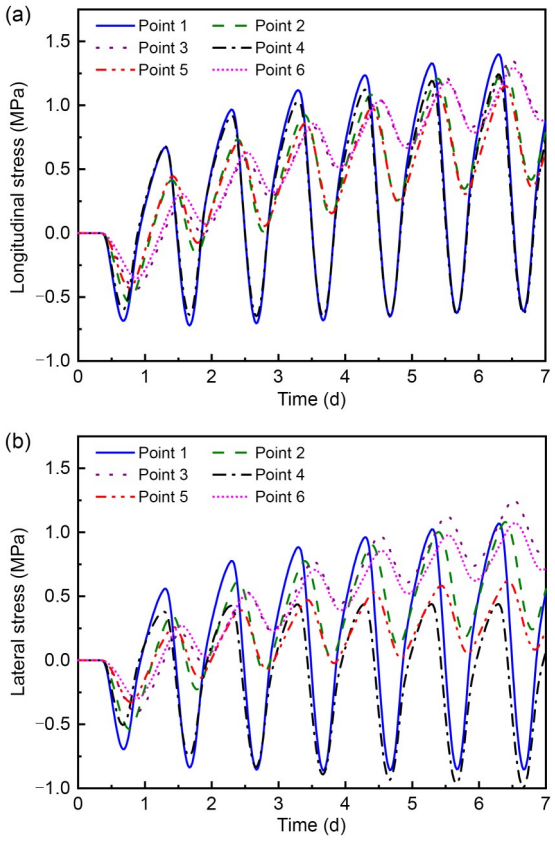

Fig. 11 Stress evolution patterns for measuring points in the track bed: (a) longitudinal stress; (b) lateral stress

layer, due to the water exchange between these elements. On the 7th day, the minimum humidity is about 92%, and some areas near the sleepers have uneven humidity levels. Due to the short exposure time, the water loss to the environment on the concrete surface layer is minimal. It can be concluded that the water consumption during hydration and the drying effect of the supporting layer are the main factors that cause the decrease of water content in the track bed. The influence of ambient temperature and relative humidity on the water content inside the track bed is essentially negligible.

3.4 Time-varying development of the stress field

The stress development of early-age concrete in the track bed is complex due to continuous changes in mechanical properties and creep coefficients during the hydration process. The stress evolution curves at points 1–6 in the track bed, as determined from the modeling, are shown in Fig. 11.

The early-age stress in the track bed changes periodically with the ambient temperature. For about the first 10 h, the concrete is in a plastic state, during which there is essentially zero effective stress in the structure for temperature and humidity deformation. Subsequently, the track bed reaches the final setting state and begins to develop strength. As the temperature increases due to hydration heat, the structure expands and enters a compressed state. The track bed then decreases in temperature and humidity, which causes the structure to enter a tensile state, thus forming a cycle of stress development. The track bed is a longitudinally-continuous structure. Its longitudinal constraints are mainly derived from the longitudinally-continuous plane strain structure, and these constraints are relatively large, which means the longitudinal stresses at the inner and outer points for the same depth are essentially the same. The lateral constraint predominantly comes from the bonding between the bonding layer and the lower supporting layer, and we find that the closer to the supporting layer (or the more inward to the track bed), the greater the lateral stress.

The cracking risk coefficient of the early-age track bed is the most intuitive parameter to evaluate structural cracking sensitivity. We take the first

principal stress component in proportion to the track bed tensile strength as the evaluation index. The time evolution of cracking risk coefficient for points 1–6 is shown in Fig. 12.

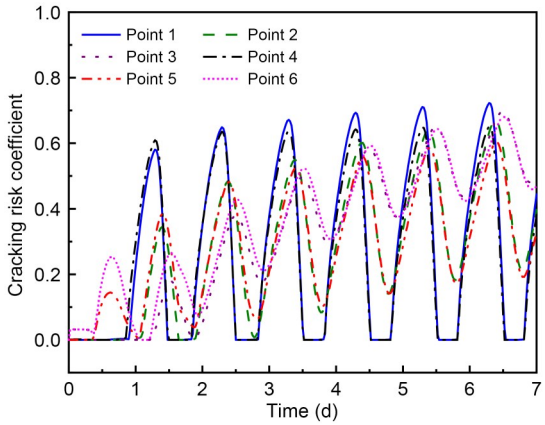

Fig. 12 Temporal evolution of track bed's cracking risk

The risk of early-age cracking in the track bed is periodic. Across the six measuring points, the cracking risks at points 1 and 4 are the highest. On day 6.25 after casting, the maximum cracking risk is about 0.72, which is because the areas closer to the surface are more susceptible to the external ambient temperature.

In Fig. 13 we investigate the cracking risk coefficients across the track bed surface for days 1.25, 2.25, and 6.25, because these are high-risk times. The arrows indicate the direction of principal stress, and three main forms of early-age cracking are illustrated (the cracking path is perpendicular to the direction of principal stress).

The distribution of risk coefficients around the sleeper is complex, especially near its corners. Moreover, the maximum cracking risk (1.00) is at the junction surface of the sleeper and the track bed, indicating that the debonding of the sleeper is likely. In terms of form, cracking form (1) develops as a splayed crack at 45° between adjacent sleepers inside the track bed, until it develops into a transverse crack; cracking form (2) develops as a 45° splayed crack between adjacent sleepers inside the track bed, until it crosses to form a longitudinal crack; cracking form (3) develops as a splayed crack at a 45° between adjacent sleepers on the outer side of the track bed, until it develops into a transverse crack.

We also study the influence of creep on cracking mechanisms in the early-age track bed, particularly considering how the creep relaxes the restrained stresses, in Section S8 of the ESM.

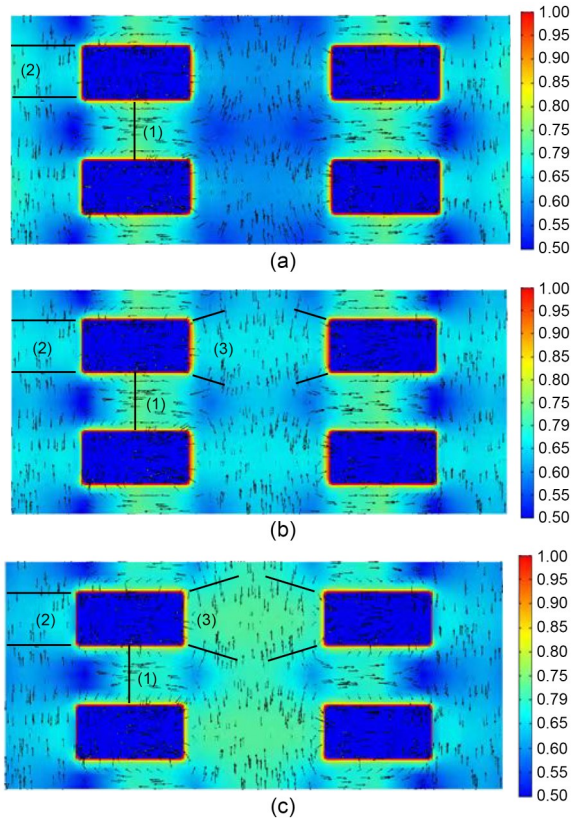

Fig. 13 Distribution diagram of cracking risk coefficients and principal stress direction on the track bed surface: (a) day 1.25; (b) day 2.25; (c) day 6.25. References to color refer to the online version of this figure

4 Risk factors and control measures for early-age track bed cracking

We use the coupled multi-field risk prediction model to systematically study the influence of material properties, environmental factors, and construction techniques on the cracking risk of the concrete track beds. This model can elucidate the influence of each factor, and we can accordingly propose more effective cracking prevention measures. The calculation details and cracking risk analysis for each factor mentioned above are detailed in Section S9 of the ESM. The formulated ranges of cracking risk are set as <0.05, 0.05–0.10, 0.10–0.15, 0.15–0.20, and >0.20, corresponding to levels 1–5 of influence, respectively. The results are shown in Table 1.

Table 1 Influence level of each factor on the cracking risk of the track bed

Influence factor		Surface		Middle		Bottom	
		Cracking risk coefficient	Influence level	Cracking risk coefficient	Influence level	Cracking risk coefficient	Influence level
Material factor	Maximum heat of hydration	0.120	3	0.210	5	0.205	5
	Peak heat release time	0.170	4	0.170	4	0.140	4
Environmental factor	Temperature difference between day and night	0.090	2	0.030	1	0.004	1
	Cooling rate	0.080	2	0.080	2	0.060	2
	Solar radiation	0.060	2	0	1	0	1
Construction factor	Molding temperature	0.050	2	0.130	3	0.155	4
	Molding time	0.070	3	0.170	4	0.140	3
	Insulation measures taken	0.120	3	0.160	4	0.180	4

From Table 1, we can say that the maximum heat of hydration is the most important risk factor across all depths (surface, middle, and bottom: 3+5+5=13), followed by the peak heat release time (i.e., hydration affinity) (4+4+4=12). While of lower influence, the molding temperature, molding time, and insulation measures also affect cracking risk.

Therefore, the risk control measures for track bed cracking, from most to least effective, are as follows: control of hydration heat, control of hydration affinity potential, enhancement of insulation measures, selection of reasonable molding time, and control of molding temperature. This order can serve as a reference to reduce cracking risk in track beds, though site feasibility and economic limitations should also be considered.

5 Conclusions

Based on the multi-field coupling theory for early-age concrete, we proposed a hydro-thermo-chemo-mechanical coupling model for early-age double-block ballastless tracks. This model was used to calculate the temporospatial distributions of hydration, temperature, humidity (chemo), and mechanical fields, and to investigate the parameters that influence cracking risk.

For the hydration field, the maximum hydration rate of the track bed occurs approximately 7.0 h after pouring, while the track bed finally sets about 9.5 h after pouring. The degree of hydration reaches 0.65 after 7 d, which is about 90% of the final hydration degree. The maximum difference ratio in the hydration rate of the track bed underneath the sleeper, influenced by temperature on the first day after pouring, is roughly 14%. In terms of the temperature field, the early-age track bed temperature is higher than the ambient temperature but presents a similar diurnal pattern. The maximum temperature of the concrete surface layer occurs approximately 16 h after pouring, which is about 15 ℃ higher than the molding temperature. In terms of the humidity (chemo) field, there are localized areas in the attachments of the double-block rail sleeper where humidity is unevenly distributed. The drying effect of the environment causes relatively little water loss, and instead, water consumption by hydration is the main factor decreasing the water content in the track bed.

When measuring the risk of early cracking in the track bed, on day 1.25, the risk coefficient of cracking at the interface between the old and new concrete around the sleeper exceeds 1. On day 6.25, the risk of cracking for the splay-shaped crack of the track bed slab (near the rail sleeper) reaches the threshold, with a risk coefficient of about 0.72. Temperature deformation is found to be the dominant factor in the development of surface stress, while humidity deformation is the main driver for the generation of tensile stress at the bottom of the track bed.

View the attachment of the thesis. In terms of material property factors, the risk of cracking increases with the maximum heat of hydration. Once the heat of hydration exceeds 430 kJ/kg, the maximum cracking risk coefficient of the surface layer exceeds the threshold (0.70). The risk of cracking and the peak heat release time are in a concave relationship, with an optimal peak heat release time occurring around 9.0 h after pouring; meanwhile, a too-high or too-low hydration rate will significantly increase the chance of

cracking. With regards to environmental and atmospheric factors, cracking risk increases linearly with the temperature difference between day and night. When this difference is 18.0 ℃, the cracking risk coefficient of the surface layer is about 0.90. The cracking risk also increases linearly with the average daily cooling rate, and the cracking risk coefficients for all layers of the track bed exceed 0.87 when the cooling rate is 0.75 ℃/d, indicating that the entire track bed has a greater cracking risk during a continuous cooling process. Solar radiation intensity has the greatest influence on the cracking risk of the surface layer, and this risk is proportional to the radiation intensity. When the solar radiation is 800 W/(m^2·K), the cracking risk coefficient of the surface layer is about 0.77. As for construction technique factors, the cracking risk increases linearly with the molding temperature, and the molding temperature should not be too high. The cracking risk is influenced by the molding time, and pouring concrete at 20:00 (given normal temperature conditions) is best for reducing the cracking risk in the track bed. The risk of cracking decreases as a convex function of the insulation coefficient, and when the insulation coefficient is larger than 0.50, the insulation layer can effectively reduce the risk of cracking in the surface layer of the track bed.

In terms of prioritizing risk control measures for the cracking of early-age track beds, the recommended measures are (in order of decreasing importance): reducing hydration heat, optimizing the peak time of heat release, enhancing insulation measures, selecting an appropriate molding time, and controlling the molding temperature.

Acknowledgments

This work is supported by the National Key R&D Program of China (No. 2021YFF0502100) and the National Natural Science Foundation of China (Nos. 52278461 and 52308467).

Author contributions

Xiao LI: conceptualization, methodology, and writing original draft. Juanjuan REN: conceptualization and funding acquisition. Shijie DENG: assistance in manuscript organization and funding acquisition. Zeyong ZHANG: data processing and assistance in manuscript organization. Xueyi LIU: writing guidance.

Conflict of interest

Xiao LI, Juanjuan REN, Shijie DENG, Zeyong ZHANG, and Xueyi LIU declare that they have no conflict of interest.

References

CEB (Comité Euro-international du Béton), 1990. CEB-FIP Model Code 1990, First Draft. CEB Bulletin D'information, Lausanne, Switzerland.

Cervera M, Faria R, Oliver JU, et al., 2002. Numerical modelling of concrete curing, regarding hydration and temperature phenomena. *Computers & Structures*, 80(18-19):1511-1521. https://doi.org/10.1016/S0045-7949(02)00104-9

de Schutter G, 1999. Degree of hydration based Kelvin model for the basic creep of early age concrete. *Materials and Structures*, 32(4):260-265. https://doi.org/10.1007/BF02479595

de Schutter G, 2002. Finite element simulation of thermal cracking in massive hardening concrete elements using degree of hydration based material laws. *Computers & Structures*, 80(27-30):2035-2042. https://doi.org/10.1016/S0045-7949(02)00270-5

de Schutter G, Taerwe L, 1996. Degree of hydration-based description of mechanical properties of early age concrete. *Materials and Structures*, 29(6):335-344. https://doi.org/10.1007/BF02486341

Du MY, 2015. Thermo-Hygro-Mechanical Model of Early-Age Concrete Based on Micro-Pore Structure Evolution. MS Thesis, Zhejiang University, Hangzhou, China (in Chinese).

Gawin D, Pesavento F, Schrefler BA, 2006. Hygro-thermo-chemo-mechanical modelling of concrete at early ages and beyond. Part I: hydration and hygro-thermal phenomena. *International Journal for Numerical Methods in Engineering*, 67(3):299-331. https://doi.org/10.1002/nme.1615

Hu RP, Zhang RL, Wang MS, et al., 2018. Experimental study on the cracking of concrete about the high speed railway in big temperature difference area of Gobi. *Bulletin of the Chinese Ceramic Society*, 37(6):2042-2047 (in Chinese). https://doi.org/10.16552/j.cnki.issn1001-1625.2018.06.041

Künzel HM, 1995. Simultaneous Heat and Moisture Transport in Building Components. One- and Two-Dimensional Calculation Using Simple Parameters. Fraunhofer IRB Verlag Suttgart.

Miao CW, 2018. Early shrinkage cracking of modern concrete and its inhibiting technology. *Journal of Xuzhou Institute of Technology (Natural Sciences Edition)*, 33(3): 1-8 (in Chinese). https://doi.org/10.15873/j.cnki.jxit.000228

MOHURD (Ministry of Housing and Urban-Rural Development of the People's Republic of China), 2004. Code for Design of Concrete Structures, GB 50010-2002. National Standards of the People's Republic of China (in Chinese).

Ren JJ, Deng SJ, Zhang KY, et al., 2021. Design theories and maintenance technologies of slab tracks for high-speed railways in China: a review. *Transportation Safety and Environment*, 3(4):tdab024. https://doi.org/10.1093/tse/tdab024.

Ren JJ, Zhang Q, Zhang YC, et al., 2023. Evaluation of slab

track quality indices based on entropy weight-fuzzy analytic hierarchy process. *Engineering Failure Analysis*, 149:107244. https://doi.org/10.1016/j.engfailanal.2023.107244

van Breugel K, 1995. Numerical simulation of hydration and microstructural development in hardening cement-based materials: (II) applications. *Cement and Concrete Research*, 25(3):522-530. https://doi.org/10.1016/0008-8846(95)00041-A

Zhang J, Hou DW, Sun W, 2010. Experimental study on the relationship between shrinkage and interior humidity of concrete at early age. *Magazine of Concrete Research*, 62(3):191-199. https://doi.org/10.1680/macr.2010.62.3.191

Zhang J, Gao Y, Wang ZB, 2013. Evaluation of shrinkage induced cracking performance of low shrinkage engineered cementitious composite by ring tests. *Composites Part B: Engineering*, 52:21-29. https://doi.org/10.1016/j.compositesb.2013.03.012

Electronic supplementary materials

Sections S1–S9, Tables S1–S4, Figs. S1–S12